Electrical Power and Energy Systems 49 (2013) 234–242

Contents lists available at SciVerse ScienceDirect

Electrical Power and Energy Systems

journal homepage: www.elsevier.com/locate/ijepes

Optimal tracking and robust power control of the DFIG wind turbine

S. Abdeddaim *, A. Betka

Laboratoire de Genie Electrique de Biskra (LGEB), Electrical Engineering Department, University of Biskra, Biskra 07000, Algeria

ARTICLE INFO

Article history:
Received 16 March 2011
Received in revised form 9 December 2012
Accepted 24 December 2012
Available online 24 February 2013

Keywords:
Wind turbine
Doubly Fed Induction Generator (DFIG)
Power control
Sliding mode control
Fuzzy MPPT algorithm

ABSTRACT

In the present paper, an optimal operation of a grid-connected variable speed wind turbine equipped with a Doubly Fed Induction Generator (DFIG) is presented. The proposed cascaded nonlinear controller is designed to perform two main objectives. In the outer loop, a maximum power point tracking (MPPT) algorithm based on fuzzy logic theory is designed to permanently extract the optimal aerodynamic energy, whereas in the inner loop, a second order sliding mode control (2-SM) is applied to achieve smooth regulation of both stator active and reactive powers quantities. The obtained simulation results show a permanent track of the MPP point regardless of the turbine power-speed slope moreover the proposed sliding mode control strategy presents attractive features such as chattering-free, compared to the conventional first order sliding technique (1-SM).

1. Introduction

During the last decades, especially after the oil crisis in the 1970s, global interest for clean and renewable energy sources has been growing intensively. Wind energy in particular, has received a strong impulse, reflected in great technology advances regarding reliability, cost-efficiency and integration to the grid of the wind energy conversion systems (WECSs). Wind turbines generate about 1.5% of the word electricity consumption, with an installed capacity of 121 GW by the end of 2008 comprising more than 70 countries [1].

These wind turbines are all based on variable speed operation using a Doubly Fed Induction Generator (DFIG) or a direct driven synchronous generator (without gearbox).

The doubly fed induction generator is used in several wind energy conversion systems. This machine has proven its efficiency due to qualities such as robustness, cost and simplicity. It offers several advantages including variable speed operation (±33% around the synchronous speed), and four-quadrant active and reactive power capabilities Such system also results in lower converter cost and lower power losses compared to a system based on a fully fed synchronous generator with full-rated converter. Moreover, the generator is robust and requires little maintenance [2–9].

The control law of the converter can be applied in order to extract maximum power of the wind turbine for differents wind speeds.

Many papers have been presented with different control schemes of DFIG. These control schemes are generally based on vector control concept (with stator flux or voltage orientation) associated with classical controllers [10–16].

With the improvements technologies in materials, power electronics and blade design, classical controllers for WECS can be updated by the development of more efficient strategies based on modern control techniques such as: fuzzy logic control [17–19], robust control [20–22], adaptive control [23] and sliding-mode control [24–27].

Among these control strategies, sliding mode (SM) control emerges as an especially suitable option to deal with variable speed operating WECS. This control technique has proven to be very robust with respect to system parameter variations and external disturbances.

In this paper, an optimal operation of a grid-connected variable speed wind turbine, based on a doubly fed induction generator is presented. The proposed control algorithms focus two main goals: a permanent track of the available maximum wind power, and a smooth regulation of the stator active and reactive powers exchanges between the machine and the grid.

In Section 2, explicit models of the different sub-systems are described. In Section 3, the proposed control algorithms are detailed precisely, while in Section 4 simulation results are presented and discussed.

2. System description and modeling

The topology of the wind energy conversion system (WECS) under consideration in this paper is depicted in Fig. 1. It is constituted

* Corresponding author.
E-mail addresses: s_abdeddaim@yahoo.fr (S. Abdeddaim), betkaachour@gmail.com (A. Betka).

0142-0615/$ - see front matter © 2013 Elsevier Ltd. All rights reserved.
http://dx.doi.org/10.1016/j.ijepes.2012.12.014

Nomenclature

V_w	wind speed, m s^{-1}	P_s, Q_s	active and reactive statoric powers, W (Var)
ρ	air density, kg m^{-3}	T_{em}	DFIG torque, N m
R	rotor radius, m	d, q	synchronous reference frame index
λ	tip-speed ratio	$V_{sd,q}$	stator d–q frame voltage, V
C_P, C_T	power and torque coefficients	$V_{rd,q}$	rotor d–q frame voltage, V
P_a	aerodynamic power, W	$I_{sd,q}$	stator d–q frame current, A
T_a	aerodynamic torque, N m	$I_{rd,q}$	rotor d–q frame current, A
Ω_t	aeroturbine rotor speed, rad s^{-1}	$\varphi_{sd,q}$	stator d–q frame flux, Wb
Ω_m	generator speed, rad s^{-1}	$\varphi_{rd,q}$	rotor d–q frame flux, Wb
Ω_s	synchronous generator speed, rad s^{-1}	R_s, R_r	stator and rotor Resistances, Ω
f	turbine total external damping, N m rad^{-1} s	L_s, L_r	stator and rotor Inductances, H
J	turbine total inertia, kg m^2	L_m	mutual inductance, H
G	gearbox ratio;	σ	leakage coefficient,
f_t, f_g	rotor and DFIG external damping, N m rad^{-1} s	ω_s, ω_r	synchronous speed and Angular speed, rad s^{-1}
J_t, J_g	rotor and DFIG inertia, kg m^2	s	generator slip

of a small scale windmill and a Doubly Fed Induction Generator (DFIG) coupled to a three phase grid.

In such configuration, the stator winding is directly connected to the grid, whereas, two converters are inserted between the rotor side and the utility grid to permit a power exchange between the grid and the machine in sub-synchronous speed. So the grid side converter (GSC) works as a rectifier, and the rotor side converter (RSC) operates to control the DFIG for independent control of active/reactive powers quantities.

In the case studied in this paper, two operation modes are distinguished: when the aerodynamic power is not enough to reach the synchronous speed, the system operates at mode 1: maximum power extraction, whereas, if the wind speed exceeds the rated value, the system switches to mode 2: power limitation, which leads the DFIG to provide its rated power below synchronous speed.

The models of the different components of the wind-turbine generation system are described below:

2.1. Wind turbine modeling

The aerodynamic power captured by the aeroturbine rotor is given by [28],

$$P_a = 0.5\rho\pi R^2 V_w^3 C_P(\lambda,\beta) \tag{1}$$

C_P is the power coefficient which is a nonlinear function of the tip speed ratio (TSR) λ

$$C_P\ (\lambda) = a_0 + a_1\lambda + a_2\lambda^2 + a_3\lambda^3 + a_4\lambda^4 + a_5\lambda^5 \tag{2}$$

The TSR is defined as the ratio between the linear blade tip speed and the wind speed, expressed as:

$$\lambda = \frac{R\Omega_t}{V_w} \tag{3}$$

Then the aerodynamic torque is given by

$$T_a = \frac{P_a}{\Omega_t} = 0.5\rho\pi R^3 V_w^2 C_T(\lambda,\beta) \tag{4}$$

where

$$C_T(\lambda,\beta) = \frac{C_P(\lambda,\beta)}{\lambda} \tag{5}$$

The $C_p(\lambda)$ characteristic is illustrated in Fig. 2. This figure indicates that there is one specific λ_{opt} at which the turbine is most efficient. Normally a variable speed wind turbine follows the C_{pmax} to capture the maximum power up to the rated speed by varying the rotor speed to keep the system at λ_{opt}.

Fig. 3 shows the power rotational speed curves of 7.8 kw wind turbine considered in the present paper under different wind speeds. The dotted line indicates the optimal power points P_{aopt} where the C_P coefficient is kept at its maximum value.

If a perfectly rigid low-speed shaft is assumed, a single mass model of the turbine may be considered [28].

$$J\dot{\Omega}_t + f\Omega_t = T_a - GT_{em} \tag{6}$$

where

$$J = J_t + G^2 J_g$$

$$f = f_t + G^2 f_g$$

$$G = \frac{\Omega_m}{\Omega_t}$$

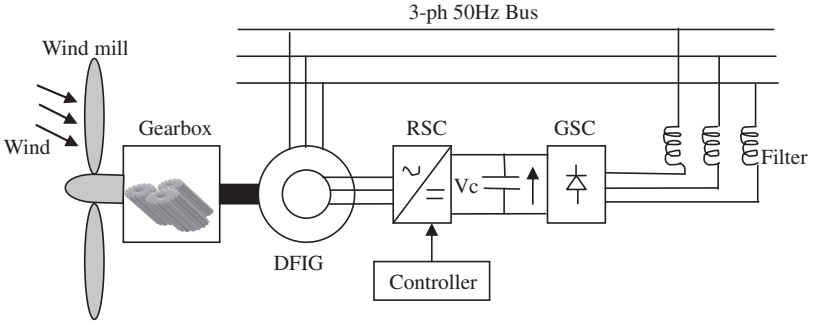

Fig. 1. Block diagram of conventional wind generator with a DFIG.

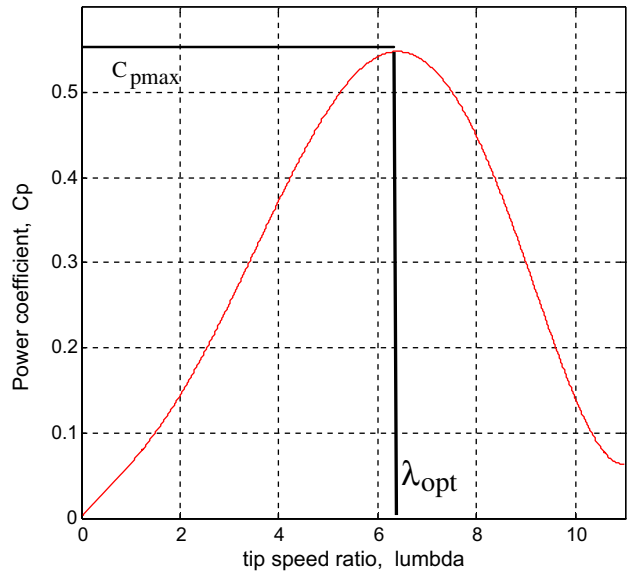

Fig. 2. Power versus tip speed ratio.

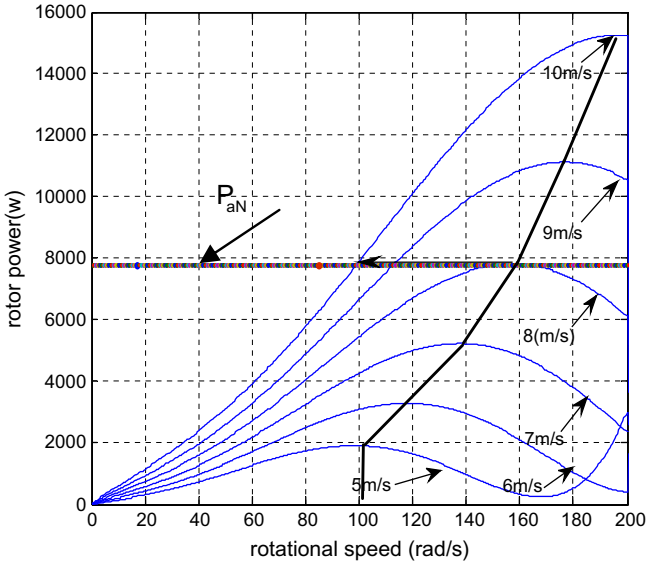

Fig. 3. Rotor power versus rotational speed of generator.

2.2. DFIG modeling

The d–q model in the arbitrary reference frame is expressed as follows [29]:

$$V_s = R_s I_s + \frac{d\varphi_s}{dt} + j\omega\varphi_s \tag{7}$$

$$V_r = R_r I_r + \frac{d\varphi_r}{dt} + j(\omega - \omega_r)\varphi_r \tag{8}$$

$$V_s = V_{sd} + jV_{sq}, V_r = V_{rd} + jV_{rq} \tag{9}$$

The stator and rotor flux are given by:

$$\varphi_s = \varphi_{sd} + j\varphi_{sq}, \quad \varphi_r = \varphi_{rd} + j\varphi_{rq} \tag{10}$$

$$\varphi_{sd} = L_s I_{sd} + L_m I_{rd}, \quad \varphi_{sq} = L_s I_{sq} + L_m I_{rq} \tag{11}$$

$$\varphi_{rd} = L_r I_{rd} + L_m I_{sd}, \quad \varphi_{rq} = L_r I_{rq} + L_m I_{sq} \tag{12}$$

Stator and rotor variables are both referred to the stator reference park frame. With this orientation, the d-component of the stator flux is equal to the total flux whereas the q-component of the stator flux is null. In this approach, decoupled control between the stator active and reactive powers is obtained.

Assuming that the resistance of the stator windings (R_s) is neglected and referring to the chosen reference frame, the voltage and the flux equations of the stator winding can be simplified in steady state as follows:

$$V_{sd} = 0, V_{sq} = \omega_s\varphi_{sd} \tag{13}$$

$$\varphi_s = L_s I_{sd} + L_m I_{rd}, \quad \varphi_{sq} = 0 \tag{14}$$

$$V_{rd} = R_r I_{rd} + \sigma L_r \frac{dI_{rd}}{dt} - s\omega_s\sigma L_r I_{rq} \tag{15}$$

$$V_{rq} = R_r I_{rq} + \sigma L_r \frac{dI_{rq}}{dt} + s\omega_s\sigma L_r I_{rd} + s\omega_s\left(\frac{L_m}{L_s}\right)\varphi_{sd} \tag{16}$$

$$\varphi_{rd} = \left(\frac{L_m}{L_s}\right)\varphi_{sd} + \sigma L_r I_{rd}, \quad \varphi_{rq} = \sigma L_r I_{rq} \tag{17}$$

where: $\sigma = 1 - \frac{L_m^2}{L_s L_r}$ From (14), the equations linking the stator currents to the rotor currents are deduced below

$$I_{sd} = \frac{\varphi_s}{L_s} - \frac{L_m}{L_s} I_{rd} \tag{18}$$

$$I_{sq} = -\frac{L_m}{L_s} I_{rq} \tag{19}$$

The active and reactive powers at the stator side of DFIG are defined by:

$$P_s = (V_{sd}I_{sd} + V_{sq}I_{sq}) \tag{20}$$

$$Q_s = (V_{sq}I_{sd} - V_{sd}I_{sq}) \tag{21}$$

Replacing the stator currents by their expressions given in (18) and (19), the equations of the active and reactive powers at the stator side of DFIG are given by:

$$P_s = -\frac{L_m}{L_s} V_{sq} I_{rq} \tag{22}$$

$$Q_s = V_{sq}\frac{L_m}{L_s}\left(\frac{\varphi_s}{L_m} - I_{rd}\right) \tag{23}$$

Due to the constant stator voltage, the stator active and reactive powers are controlled by means of I_{rq} and I_{rd} respectively.

3. The variable speed control strategy

3.1. Control structure

The wind turbine electric system time responses are much faster than those of the others parts of the WECS. This makes it possible to dissociate the generator and the aeroturbine control designs and thus define a cascaded control structure around two sub-system control:

- The power sub-system control concerns the electric generator via the power converter.
- The wind sub-system control concerns the aeroturbine that provides the reference inputs of the power sub-system control. Thereafter, these two control levels will be considered separately as seen in Fig. 4.

3.2. Wind sub-system control

The two possible modes of control are as follows.

- Mode 1: tracking mode It corresponds to periods of sufficient wind power to satisfy the total demand, this situation is maintained until both the rated power and synchronous speed are attained (zone2) Fig. 5.

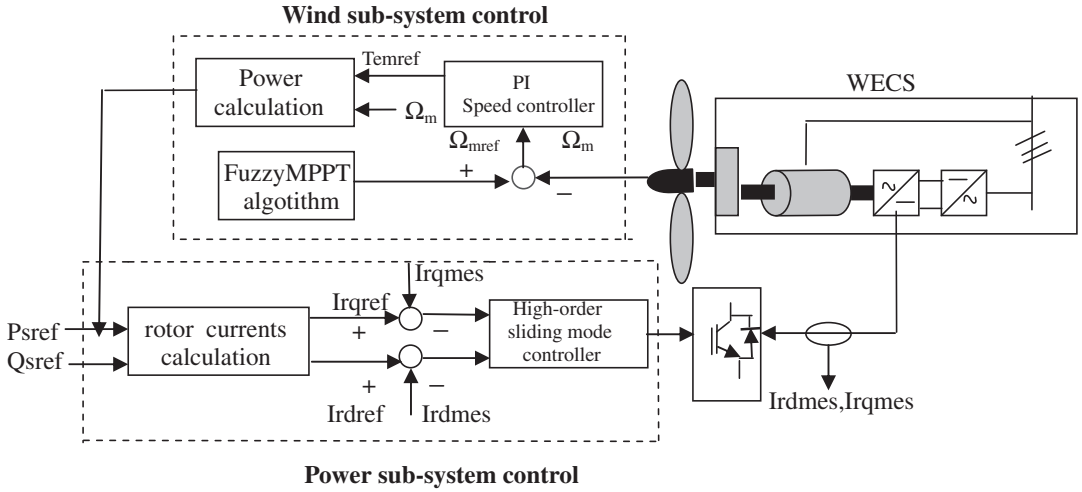

Fig. 4. Block-diagram of the whole system.

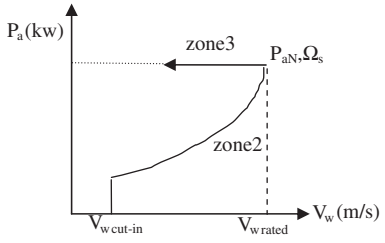

Fig. 5. Operating zones of the wind turbine.

- Mode 2: power regulation Up to rated wind speed (8 m s^{-1}), the control is designed, so that the extracted power and the rotational speed do not exceed their nominal values (zone3) Fig. 5.

3.2.1. The fuzzy MPPT controller

In order to tracking an optimal rotor speed reference, without measuring the wind speed and without the knowledge of the turbine characteristics because the use of wind speed sensor to measure the wind speed adds to a system a cost and presents some difficulties in practical implementation.

A control which is based on MPPT fuzzy controller (FLCMPPT) is developed in this paper.

The proposed FLC measures the power and rotational speed and then perturbs the operating speed by an optimal increment ($\Delta\Omega_{mref}$) so the resulting power turbine change. The power variation (ΔP_a) is either in the positive direction or in the negative one; the speed variation ($\Delta\Omega_m$) can be also small or large. From these judgements, the reference rotational speed variation ($\Delta\Omega_{mref}$) increases or decreases in a small or respectively large way in the direction which makes it possible to increase the power P_a.

The control rules are indicated in Table 1: with (ΔP_a) and ($\Delta\Omega_m$) as inputs, while ($\Delta\Omega_{mref}$) represent the output. These inputs and output variables are expressed in terms of linguistic variables (such as BN (big negative), MN (means negative), SN (small negative), Z (zero), SP (small positive), MP (means positive), BP (big positive)).

From these linguistic rules, the FLC proposes a variation of the reference speed ($\Delta\Omega_{mref}$) according to:

$$\Delta P_a = P_a[k] - P_a[k-1] \quad (24)$$

$$\Delta\Omega_m = \Omega_m[k] - \Omega_m[k-1] \quad (25)$$

$$\Omega_{mref}[k] = \Omega_m[k-1] + \Delta\Omega_{mref}[k] \quad (26)$$

where $P_a[k]$ and $\Omega_m[k]$ are the rotor power and rotational speed at sampled times (k), and $\Omega_{mref}[k]$ is the instant of reference speed.

The fuzzy logic controller structure is shown in Fig. 6, where K1, K2 and K3 are adaptive gains.

The bloc fuzzy logic controller includes three functional blocks: fuzzification, fuzzy rule algorithm, and defuzzification.

The membership functions of inputs variables (ΔP_a) and ($\Delta\Omega_m$) are triangular and have seven fuzzy subsets. Seven fuzzy subsets are also considered for the output variable $\Delta\Omega_{mref}$.

The fuzzy inference is carried out by using Sugeno's method [30,31], and the defuzzification uses the center of gravity to compute the output of this FLC.

As explained previously, the FLC optimises the reference speed Ω_{mref} for maximum power tracking. This speed represents a positive input (reference) of the PI controller, which performs the speed control in steady state. The PI loop operates with a fast rate and provides fast response and overall system stability.

Table 1
Fuzzy rule table.

$\Delta\Omega_m$	Δ Pa						
	BN	MN	SN	Z	SP	MP	BP
BN	BP	BP	MP	Z	MN	BN	BN
MN	BP	MP	SP	Z	SN	MN	BN
SP	MP	SP	SP	Z	SN	SN	MN
Z	BN	MN	SN	Z	SP	MP	BP
SP	MN	SN	SN	Z	SP	SP	MP
MP	BN	MN	SN	Z	SP	MP	BP
BP	BN	BN	MN	Z	MP	BP	BP

3.2.2. Power limit

Above the rated wind speed (Mode 2), the control must limit the extracted power in the tolerable range between P_{aN}–1.1 P_{aN} and the rotational speed in the stable operation mode (30–100%Ω_s), so when the extracted power increases over the nominal value, the control circuit reduces the reference speed Fig. 7 to prevent steady-state high power amounts. A speed controller circuit added to the previous FLCMPPT design, the sensed stator power as a feedback. When the power exceeds the maximum value, the reference speed must be reduced by the amount, K4 ($P_{ames} - P_{aN}$) [32].

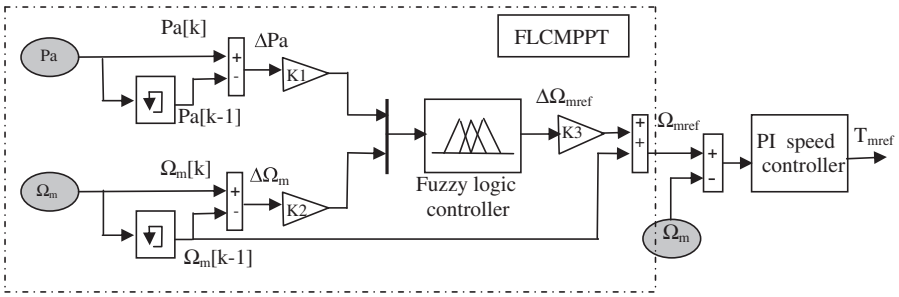

Fig. 6. Structure of MPPT fuzzy controller.

$$\Omega_{mrefnew} = \Omega_{mref} - \Delta\Omega_m$$

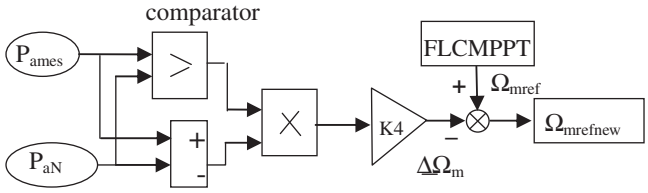

Fig. 7. Detailed block diagram of the power limit.

where

$$K4 = \frac{\Delta P}{\Delta \Omega}$$

$$\Delta P = 1.1P_{aN} - P_{aN}$$

$$\Delta \Omega = \Omega_s - 0.3\Omega_s$$

the new reference speed $\Omega_{mrefnew}$ is then given by:

$$\Omega_{mrefnew} = \Omega_{mref} - \quad \Delta\Omega_m \tag{27}$$

3.3. Power sub-system control

A common practice in addressing DFIG control problem is to use the linearisation approach [33,34]. However, due to inevitable inherent uncertainties in WECS based on DFIG, such control methods come at the price of poor system performance and low reliability [35]. Hence the need for nonlinear and robust control to take into account these control problems. In this context, sliding mode control seems to be an interesting approach.

3.3.1. High order sliding mode controller design

The first order sliding mode control (1-SM) is an effective nonlinear robust control.

However, a few problems arise in some practical applications, such as chattering effect and undesirable mechanical stresses.

The second order sliding mode (2-SM) algorithm synthesizes a discontinuous control which makes the surface and its derivative nul with continuous control, therefore reducing chattering and avoiding strong mechanical efforts while preserving (1-SM) advantages [36].

To ensure the DFIG active and reactive stator powers convergence, the d–q rotor currents references are linked to the optimal active and reactive stator powers as follows:

$$I_{rqref} = -\frac{L_s}{L_m V_s} P_{sref} \tag{28}$$

$$I_{rdref} = \frac{V_s}{\omega_s L_m} \tag{29}$$

The optimal reactive power is set to zero to ensure a unity power factor operation of the studied wind turbine: $Q_{sref} = 0$. Whereas the optimal active power P_{sref} can be written with neglected losses as:

$$P_{sref} \approx \quad P_{aopt}. \tag{30}$$

The block diagram of the second order sliding mode control applied to the DFIG is illustrated in Fig. 8 [37].

Let us consider the following surfaces:

$$\sigma_d = I_{rd} - I_{rdref} \tag{31}$$

$$\sigma_q = I_{rq} - I_{rqref} \tag{32}$$

Then we have

$$\dot{\sigma}_d = \frac{1}{L_r \sigma} V_{rd} + \frac{1}{L_r \sigma}(-R_r I_{rd} + g\omega_s L_r \sigma I_{rq}) - I_{rdref} \tag{33}$$

$$\dot{\sigma}_q = \frac{1}{L_r \sigma} V_{rq} + \frac{1}{L_r \sigma}\left(-R_r I_{rq} - g\omega_s L_r \sigma I_{rd} - g\omega_s \varphi_s \left(\frac{L_m}{L_s}\right)\right) - \dot{I}_{rqref} \tag{34}$$

If we define the functions G_1 and G_2 as follows:

$$G_1 = \frac{1}{L_r \sigma}(-R_r I_{rd} + g\omega_s L_r \sigma I_{rq}) - \dot{I}_{rdref}$$

$$G_2 = \frac{1}{L_r \sigma}\left(-R_r I_{rq} - g\omega_s L_r \sigma I_{rd} - g\omega_s \varphi_s \left(\frac{L_m}{L_s}\right)\right) - \dot{I}_{rqref}$$

Thus:

$$\ddot{\sigma}_d = \frac{1}{L_r \sigma} \dot{V}_{rd} + \dot{G}_1 \tag{35}$$

$$\ddot{\sigma}_q = \frac{1}{L_r \sigma} \dot{V}_{rq} + \dot{G}_2 \tag{36}$$

The control algorithm proposed which is based on super twisting algorithm (ST) has been introduced by Levant [38]. The second order sliding mode controllers contain two parts:

where

$$V_{rd} = u_1 + u_2 \tag{37}$$

with

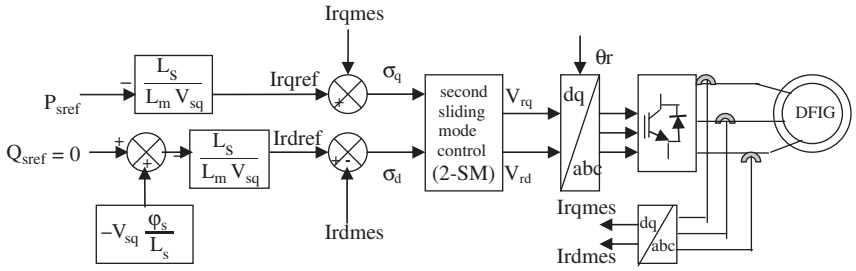

Fig. 8. Block diagram of a second sliding mode control applied to the DFIG.

$$\dot{u}_1 = -\alpha_1 \mathrm{sign}(\sigma_d)$$
$$u_2 = -\theta_1 |\sigma_d|^{0.5} \mathrm{sign}(\sigma_d)$$

and

$$V_{rq} = w_1 + w_2 \tag{38}$$

with

$$\dot{w}_1 = -\alpha_2 \mathrm{sign}(\sigma_q)$$
$$w_2 = -\theta_2 |\sigma_q|^{0.5} \mathrm{sign}(\sigma_q)$$

In order to ensure the convergence of the sliding manifolds to zero in finite time, the constants α_i and θ_i can be chosen as follows:

$$\alpha_i > \frac{\mu_i}{L_r \sigma}$$
$$\theta_i \geqslant \frac{4\mu_i(\alpha_i + \mu_i)}{L_r^2 \sigma^2 (\alpha_i - \mu_i)}$$
$$|\dot{G}_i| < \mu_i; \quad i = 1,2 \tag{39}$$

4. Simulations results

The simulation results are carried out using Matlab–Simulink package, under a wind speed profile of (8 m/s) mean value, as depicted in Fig. 9a and the rated system parameters are given in Appendix A.

It can be seen in Fig. 9. b that up to the rated wind speed (8 m/s), the MPPT controller ensures the tracking of the optimum power points MPPT (mode 1), by maintaining the power coefficient to its maximum value Cpmax (0.54); whereas above the rated wind speed, the power coefficient is reduced accordingly to (mode 2), to perform constant power operation (power limitation).

In Fig. 10 are displayed the active and reactive powers at the stator side of the DFIG, controlled via the proposed high order sliding mode controller (2-SM), while, in a comparative way, Fig. 11, describes these quantities under the conventional first order sliding mode control (1-SM). One can conclude that, under the super-twisting control algorithm, the stator power amounts track their references values with smooth profiles, with chattering-free. On the other hand, in Fig. 11 undesirable surging phenomena chattering are easily remarked. In addition, to see the efficiency of the proposed control strategy, Table 2 presents the results of the following tracking indices:

1. The Integral of absolute error: IAE, given by: $\mathrm{IAE} = \int_0^t |e(t)|dt$.
2. The Integral of square error: ISE, as: $\mathrm{ISE} = \int_0^t e^2(t)dt$.

One can easily conclude, that the suggested control technique submits low tracking indices over the wind speed profile, which proves its performance, while compared to the 1-SM strategy.

Fig. 12a shows both the DFIG speed and its reference, while Fig. 12. b gives the speed tracking error. Two remarks can be extracted:

1- In mode 1, the DFIG speed tracks satisfactory its optimum reference, provided by the FLC algorithm with negligible error (Fig. 12b).

2- In mode 2, as the power limitation circuit described above, the speed values are bounded in the tolerable range under constant power, a reduction of the machine's speed is observed. Consequently, the DFIG releases its rated power with a speed range from 450 to 1500 rpm.

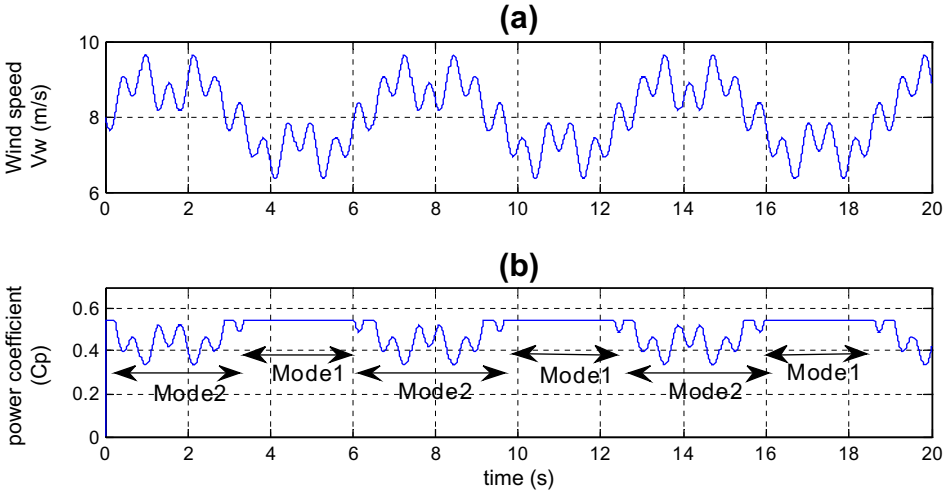

Fig. 9. Simulation waveforms of (a) wind speed profile of (8 ms^{-1}) mean value, (b) power coefficient Cp.

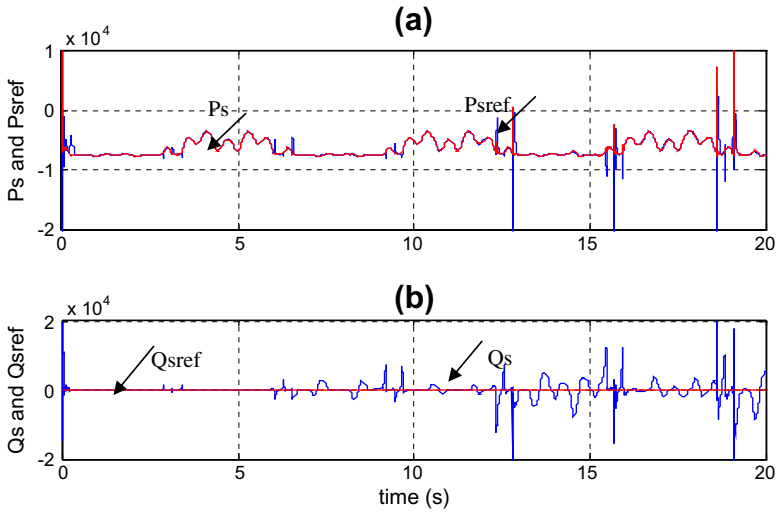

Fig. 10. Simulation waveforms of the proposed (2-SM) control (a) waveforms of the reference and measured active powers at stator side of the DFIG (Psref, Ps) and (b) waveforms of the reference and measured reactive powers at stator side of the DFIG (Qsref, Qs).

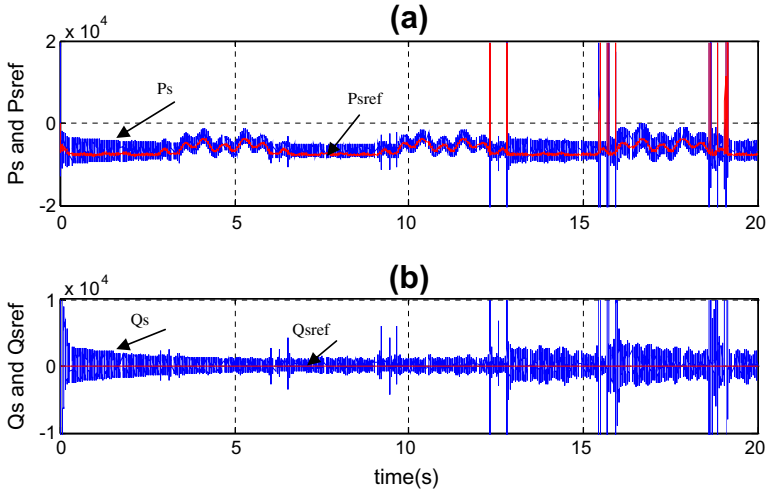

Fig. 11. Simulation waveforms of (1-SM) control: (a) waveforms of the reference and measured active powers at stator side of the DFIG (Psref, Ps) and (b) waveforms of the reference and measured reactive powers at stator side of the DFIG (Qsref, Qs).

Table 2
Performance indices.

	IAEd	IAEq	ISEd	ISEq
1-SM	6.83	7.64	6.289	7.983
2-SM	3.92	2.16	0.859	1.48

Fig. 13 displays respectively the rotor current waveform and the d–q sliding surfaces. It can be seen, that the rotor is supplied with variable low frequency signals according to wind speed variations. In addition, after a brief time (convergence mode), the two axes sliding surfaces reach their steady-state values (zero) smoothly.

Finally, Fig. 14 displays, a sample waveform of the DFIG stator current and voltage, between 2 s and 2.1 s. It can be seen that the phase angle is kept at 180°, which proves that the DFIG machine performs as generator, and no reactive power is provided to the grid, as can be checked on Fig. 10b.

5. Conclusion

The DFIG is nowadays a popular choice for wind energy conversion systems. This popularity is mostly due to its ability for large variable speed drive. Such system also results in lower converter cost and lower power losses compared to a system based on a fully fed synchronous generator with full-rated converter.

In this paper, a complete system to produce electrical energy using DFIG is presented. The stator is directly connected to the grid and the rotor is connected to the utility by the way of two converters (machine inverter and grid rectifier). A cascaded control algorithms where properly designed to ensure the optimal operation of the whole system. In the outer loop, a fuzzy logic controller was designed to extract the maximum aerodynamic power up to the rated power, regardless of the turbine power-speed slope. If the wind power exceeds the rated value, the system switches to power regulation mode, via the power limitation circuit. In the inner loop, the described high order sliding mode controller has been designed to control the active and reactive powers exchanged between the machine and the grid, through the machine inverter. The obtained simulation results show that the system switches with flexibility between the "Tracking mode" and the "Power regulation mode" without synchronous speed overshoot. On the other hand, the stator power quantities provided by the 2-SM strategy show

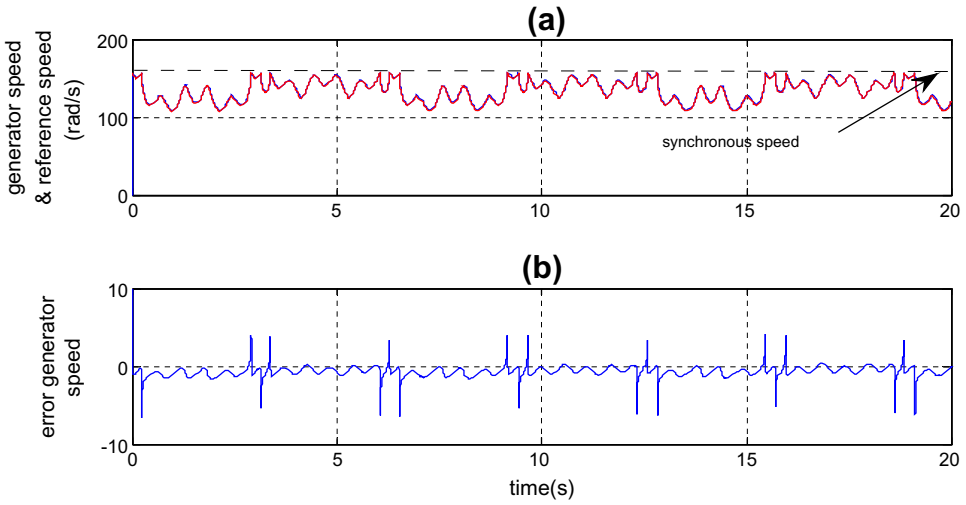

Fig. 12. Simulation results of (a) generator speed with the reference speed and (b) error speed.

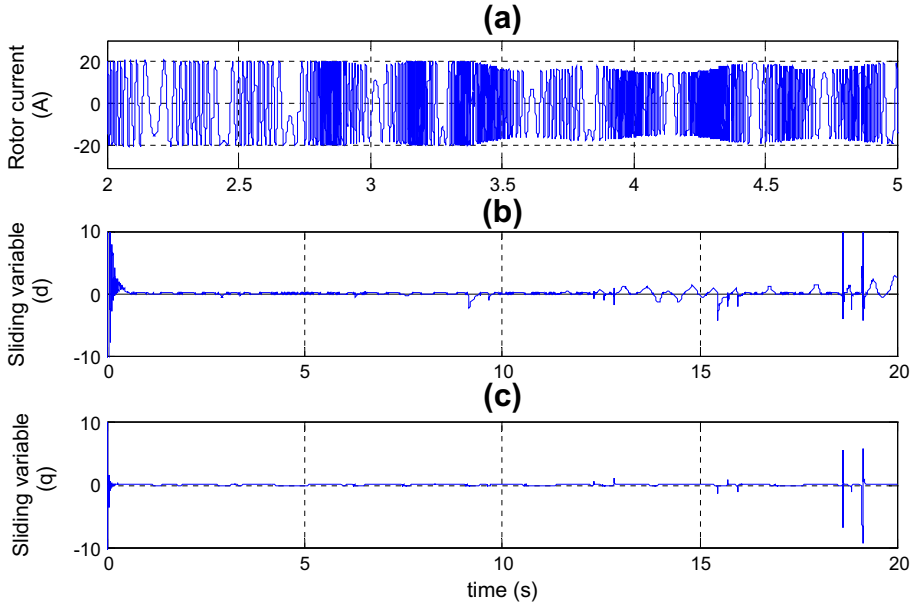

Fig. 13. Simulation results of (a) Rotor current of the DFIG and (b) Sliding variables $\sigma_d(t)$,$\sigma_q(t)$.

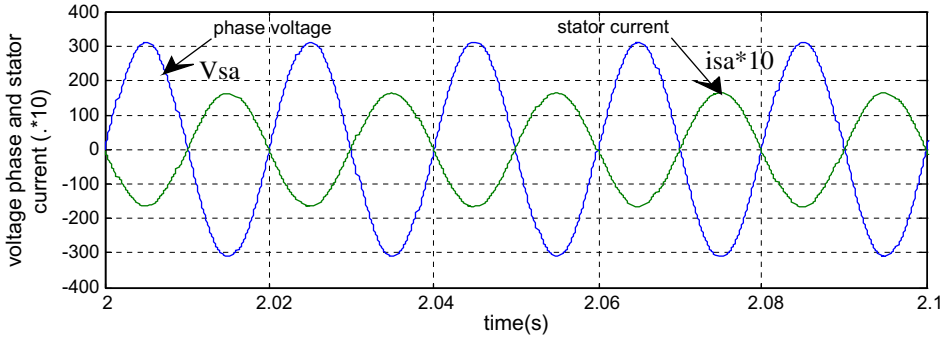

Fig. 14. DFIG Stator voltage and stator current waveforms.

smooth waveforms, with good tracking indices. Consequently, undesirable mechanical stresses and the chattering phenomena in the case of 1-SM control are avoided.

Appendix A

See Table A.1.

Table A.1
DFIG and turbine models parameters.

Parameters	Value
A. DFIG data	
Rated power	7.5 (kw)
Rated line voltage	220 (V)
Grid frequency	50 (Hz)
R_s	0.455 (Ω)
R_r	0.62 (Ω)
L_s	0.084 (H)
L_r (refer to stator)	0.081 (H)
Lm (refer to rotor)	0.078 (H)
Moment of inertia, J	0.3125 (kg m^2)
Friction coefficient, f	$6.73.10^{-3}$ (N m s^{-2})
Number of poles	4
B. Wind turbine data	
Rated power P_{aN}	7.8 (kw)
a_0	0.001
a_1	6.38×10^{-2}
a_2	-9.40×10^{-2}
a_3	9.86×10^{-3}
a_4	-17.375×10^{-4}
a_5	7.956×10^{-5}
R	3.80 (m)
Rated wind speed	8 (m s^{-1})
Cut-in speed	5 (m s^{-1})

References

[1] World wind energy report 2008, report. Charles-de-Gaulle-Str. 5, Bonn, Germany: World Wind Energy Association; 2009.
[2] M.E.H. Benbouzid et al, The state of the art of generators for wind energy conversion systems. In Proceedings of ICEM'06, Chania, Crete Island, Greece, September; 2006.
[3] Carrasco JM et al. Power-electronic systems for the grid integration of renewable energy sources: A survey. IEEE Trans Ind Electron 2006;53(4): 1002–16.
[4] Heier S. Grid integration of wind energy conversion systems. England: John Wiley & Sons Ltd.; 1998.
[5] Datta R, Ranganathan VT. Variable-speed wind power generation using doubly fed wound rotor induction machine-a comparison with alternative schemes. IEEE Trans Energy Convers 2002;17(3):414–21.
[6] Muller S et al. Doubly fed induction generator systems. IEEE Indu Appl Mag 2002;8(3):26–33.
[7] Senthil Kumar N, Gokulakrishnan J. Impact of FACTS controllers on the stability of power systems connected with doubly fed induction generators. Int J Electr Power Energy Syst 2011;33(5):1172–84.
[8] Ourici Amel. Double flux orientation control for a doubly fed induction machine. Int J Electr Power Energy Syst 2012;43(01):617–20.
[9] López-Garcı'a I, Espinosa-Pérez G, Siguerdidjane H, Dòria-Cerezo A. On the passivity-based power control of a doubly-fed induction machine. Int J Electr Power Energy Syst 2013;46(in progress):303–12.
[10] Pena R, Clare JC, Asher GM. A doubly fed induction generator using back to back converters supplying an isolated load from a variable speed wind turbine. IEE Proc Electr Power Appl 1996;143(5).
[11] Poller MA. Doubly-fed induction machine models for stability assessment of wind farms. Power technology conference proceedings, vol. 3. Bologna: IEEE; 2003. 23–26.
[12] Sun T, Chen Z, Blaabjerg F. Flicker study on variable speed wind turbines with doubly fed induction wind generators. IEEE Trans Energy Convers 2005;20(4):896–905.
[13] Brekken TKA, Mohan N. control of a doubly fed induction wind generator under unbalanced grid voltage conditions. IEEE Trans Energy Convers 2007;22(1):129–35.
[14] Darengosse C, Poitiers F Machmoum M. Advanced control of a doubly-fed induction machine for variable-speed wind energy generation. In: EPE 2003, Toulouse, France, 2–4 September, Cd-ROM Proceedings; 2003.
[15] Poitiers F, Bouaouiche T, Machmoum M. Advanced control of a doubly-fed induction generator wind energy conversion. Electric Power Syst Res 2009;79:1085–96.
[16] Boyette A, Saadate S, Poure P. Direct and indirect control of a Doubly Fed Induction Generator wind turbine including a storage unit. IEEE; 2006.
[17] Godoy Simoes M, Bose BK, Spiegel RJ. Fuzzy logic based intelligent control of a variable speed cage machine wind generation system. IEEE Trans Power Electron 1997;12(1):87–95.
[18] Li H, Hu YG, Yang C, Chen Z, Ji HT, Zhao B. An improved fuzzy synthetic condition assessment of a wind turbine generator system. Int J Electr Power Energy Syst 2013;46(in progress):468–76.
[19] Algazar Mohamed M, AL-monier Hamdy, EL-halim Hamdy Abd, Salem Mohamed Ezzat El Kotb. Maximum power point tracking using fuzzy logic control. Int J Electr Power Energy Syst 2012;39(01):21–8.
[20] Uhlen K, Foss BA, Gjosaeter OB. Robust control and analysis of a wind-diesel hybrid power plant. IEEE Trans Energy Convers 1994;9(4):701–8.
[21] Kamal Elkhatib, Aitouche Abdel, Ghorbani Reza, Bayart Mireille. Robust nonlinear control of wind energy conversion systems. Int J Electr Power Energy Syst 2013;46(in progress):202–9.
[22] Chen Chiung Hsing, Hong Chih-Ming, Cheng Fu-Sheng. Intelligent speed sensorless maximum power point tracking control for wind generation system. Int J Electr Power Energy Syst 2012;42(01):399–407.
[23] Valenciaga F, Puleston PF, Mantz RJ, Battaiotto PE. An adaptive feedback linearization strategy for variable speed wind energy conversion systems. Int J Energy Res 2000;24(2):151–61.
[24] Utkin VI, Guldner J, Shi J. Sliding mode control theory in electromechanical systems. NewYork: Taylor & Francis; 1999.
[25] Evangelista C, Puleston P, Valenciaga F. Wind turbine efficiency optimization. Comparative study of controllers based on second order sliding modes. Int J Hydrogen Energy 2010;35:5934–9.
[26] Beltran B, Ahmed-Ali T, Benbouzid M. High-order sliding-mode control of variable-speed wind turbines. IEEE Trans Ind Electron 2009;56(9).
[27] Amimeur H, Aouzellag D, Abdessemed R, Ghedamsi K. Sliding mode control of a dual-stator induction generator for wind energy conversion systems. Int J Electr Power Energy Syst 2012;42(01):60–70.
[28] Boukhezzar B, Siguerdidjane H. Nonlinear control with wind estimation of a DFIG variable speed wind turbine for power capture optimization. Energy Convers Manag 2009;50:885–92.
[29] Ghennam T, Berkouk E. Back-to-back three-level converter controlled by a novel spase-vector hysteresis current control for wind conversion systems. Electric Power Syst Res 2009.
[30] Siarry P, Guely F. Fuzzy Sets Syst 1998;99(1):37–47.
[31] Lalouni S, Rekioua D, Rekioua T, Matagne E. Fuzzy logic control of stand-alone photovoltaic system with battery storage. J Power Sources 2009;193:899–907.
[32] Soler J, et al. Analog low cost maximum power point tracking PWM circuit for DC loads. In: Proceedings of the fifth IASTED Int Conf Power and Energy Syst, Benalmadena, Spain, June 15–17; 2005.
[33] Pena R et al. Sensorless control of doubly-fed induction generators using a rotor-current based MRAS observer. IEEE Trans Ind Electron 2008;55(1):330–9.
[34] Tapia G et al. Proportional-integral regulator-based approach to wind farm reactive power management for secondary voltage control. IEEE Trans Energy Convers 2007;22(2):488–98.
[35] Mirecki A et al. Architecture complexity and energy sfficiency of small wind turbines. IEEE Trans Ind Electron 2007;54(1):660–70.
[36] Bartolini G, Ferrara A, Levant A, Usai E. Variable structure systems, sliding mode and nonlinear control. Berlin/Heidelberg: Springer; 1999. ch. On second order sliding mode controllers, p. 329–85.
[37] Ben Elghali SE et al. High-order sliding mode control of DFIG-based current turbine. IEEE; 2008.
[38] Fridman L, Levant A. Sliding mode control in engineering. Higher order sliding modes. Marcel Dekker, Inc.; 2002. chapter 3, p. 53–101.